Article No. jmbi.1998.2480 available online at http://www.idealibrary.com on IDEAL J. Mol. Biol. (1999) 286, 151–162

JMB

Exhibit B

Crystal Structure of Ovine Interferon-τ at 2.1 Å Resolution

Ramaswamy Radhakrishnan[1], Leigh J. Walter[1], Prem S. Subramaniam[3] Howard M. Johnson[3] and Mark R. Walter[1,2]*

[1]*Center for Macromolecular Crystallography and*
[2]*Department of Microbiology University of Alabama at Birmingham, Birmingham AL 35294, USA*

[3]*Department of Microbiology and Cell Science, University of Florida, Gainesville FL 32611, USA*

**Corresponding author*

Ovine interferon-τ (ovIFN-τ) is a pregnancy recognition hormone required for normal embryonic development in sheep. In addition to its novel role in reproductive physiology, ovIFN-τ displays antiviral and antiproliferative activities similar to the IFN-α subtypes. To probe the structural basis for its unique activity profile, the crystal structure of ovIFN-τ has been determined at 2.1 Å resolution. The fold of ovIFN-τ is similar to the previously determined crystal structures of human IFN-α_{2b} and human and murine IFN-β, which each contain five α-helices. Comparison of ovIFN-τ with huIFN-α_{2b}, huIFN-β, and muIFN-β reveals unexpected structural differences that occur in regions of considerable sequence identity. Specifically, main-chain differences up to 11 Å occur for residues in helix A, the AB loop, helix B, and the BC loop. Furthermore, these regions are known to be important for receptor binding and biological activity. Of particular interest, a buried ion pair is observed in ovIFN-τ between Glu71 and Arg145 which displaces a conserved tryptophan residue (Trp77) from the helical bundle core. This ion pair represents a major change in the core of ovIFN-τ compared to huIFN-α_{2b}. Based on amino acid sequence comparisons, these ovIFN-τ structural features may be conserved in several human IFN-α subtypes and IFN-ω. The structure identifies potential problems in interpreting site-directed mutagenesis data on the human IFN-α family that consists of 12 proteins.

Keywords: cytokine; type I interferon; pregnancy hormone; X-ray structure; four-helix bundle

Introduction

Ovine interferon tau (ovIFN-τ) is a member of the type I interferon (IFN) family that also includes IFN-α, IFN-β, and IFN-ω (Roberts *et al.*, 1992). Originally called trophoblast protein-1, ovIFN-τ is the major secretory product of the pre-implanted sheep conceptus during days 13-21 of pregnancy (Godkin *et al.*, 1982). The high level production of ovIFN-τ during this period prevents regression of the corpus luteum (which nourishes the developing embryo) by blocking the pusatile secretion of uterine prostaglandin $F_{2\alpha}$(Roberts, 1991). Despite its novel role in the reproductive physiology of ruminants, ovIFN-τ displays antiviral, antiproliferative, and immunological activities roughly equivalent to IFN-α (Pontzer *et al.*, 1988, 1991).

The mature protein sequences of IFN-τ, as well as IFN-ω, contain 172 amino acid residues compared to 166 for IFN-α subtypes (165 for IFN-α_2) and IFN-β (Imakawa *et al.*, 1987). The six additional residues of IFN-τ and IFN-ω are located at the C terminus of the molecule. OvIFN-τ shares amino acid sequence identities of approximately 50% with human IFN-α and IFN-ω sequences, and 30% with human IFN-β. The three-dimensional type I IFN fold has been elucidated by crystal structures of human IFN-α_{2b}, and murine and human IFN-β (Radhakrishnan *et al.*, 1996; Senda *et al.*, 1995a; Karpusas *et al.*, 1997). The IFNs are members of the α-helical cytokine family which adopt a common four-helix bundle topology first observed for porcine growth hormone (Abdel-

Abbreviations used: cm, calculated mass; hu, human; IFN, interferon; MALDI, matrix assisted laser desorption/ionization; mu, murine; ov, ovine; TOF, time of flight.

E-mail address of the corresponding author: walter@onyx.cmc.uab.edu

0022-2836/99/060151–12 $30.00/0

Meguid *et al.*, 1987). The type I IFN fold is distinguished from other α-helical cytokines by the presence of a fifth helix which tightly associates with the helix bundle (Sprang & Bazan, 1993).

Cellular responses to the human type I IFNs require at least two receptor chains, IFNAR-1 and IFNAR-2 (Uzé *et al.*, 1990; Domanski *et al.*, 1995). The extracellular domain of the IFNAR-2 adopts a modular architecture consisting of tandem fibronectin type III domains (Seto *et al.*, 1995). The interface between these domains is proposed to form the IFN binding site. The IFNAR-1 chain contains four fibronectin type III domains and may bind two IFNs simultaneously. The intracellular domains of IFNAR-1 and IFNAR-2 are associated with Tyk-2 and Jak-1 kinases, respectively (Barbieri *et al.*, 1994; Colamonici *et al.*, 1996). Cell signaling is thought to occur by IFN-induced receptor oligomerization. This activates the intracellular kinases and subsequently nuclear transcription activators (STATS) that stimulate the appropriate biological responses (Pellegrini & Dusanter-Fourt, 1997). Recently, the antiproliferative activities of IFN-α on T-cells have been shown to require components of the T-cell receptor signaling pathway CD45, Lck, and ZAP-70 (Petricoin *et al.*, 1997).

Increasing evidence suggests that the different activity profiles of the IFNs are due to altered affinities for their receptors. The unique activity profile of ovIFN-τ makes it an excellent candidate for studying type I IFN receptor-ligand interactions. For example, IFN-τ and IFN-α share equivalent antiviral activities, yet IFN-α is much less effective in sustaining the lifespan of the corpus luteum (Roberts *et al.*, 1991). Additional studies have shown that unlike IFN-α, ovIFN-τ is less toxic to cells when administered *in vitro* at high concentrations (Pontzer *et al.*, 1991; Subramaniam *et al.*, 1995; Strander, 1989). Furthermore, synthetic ovIFN-τ peptides 1-37, 62-92, 119-150, and 139-172 inhibit ovIFN-τ antiviral activity on MDBK cells in a dose dependent manner (Pontzer *et al.*, 1990, 1994). However, only peptides 62-92, 119-150, and 139-172 inhibited human IFN-α antiviral activity. These data suggest that differences in receptor binding and biological activity between ovIFN-τ and human IFN-α are localized to the N terminus of the molecules. Understanding the detailed structural mechanisms of IFN receptor engagement is important, since the human type I IFNs have been shown to be effective in the treatment of approximately 15 diseases worldwide, including hairy-cell leukemia, hepatitis, Kaposi's sarcoma, and multiple sclerosis (Baron *et al.*, 1991; Nagabhushan & Giaquinto, 1995).

Based on the high degree of sequence identities of the type I IFNs, homology models of IFN-τ have been constructed using the structure of murine IFN-β (Jarpe *et al.*, 1994; Senda *et al.*, 1995a,b). Here, we report the crystallization and structure determination of ovIFN-τ at 2.1 Å resolution. Differences in receptor binding and biological activity of ovIFN-τ and IFN-α_{2b} may be correlated with the structural deviations observed in helices A, B, and E, as well as the AB and BC loops. Based on amino acid sequence analysis of the human IFN-α subtypes, structural features observed in ovIFN-τ may also be found in a subset of the human IFN-α subtypes. The structure also identifies potential problems in interpreting site-directed mutagenesis data on the human IFN-α family that consists of 12 proteins.

Results

Quality of the structure

The crystal structure of ovIFN-τ was solved by multiple isomorphous replacement and refined to 2.1 Å resolution. Molecular replacement (MR) studies using AMoRe (Navaza, 1994) with human IFN-α_{2b}, murine IFN-β, and other helical cytokines as the search models were unsuccessful. However, since ovIFN-τ contains an unpaired cysteine residue at position 86, mercury derivatives were easily identified (Table 1). The final *R*-factor for all data between 15-2.1 Å is 21.4% with a free *R*-factor of 25.0% (Table 2). Root-mean-square deviations from ideal bond lengths and angles are 0.01 Å and 1.4°, respectively. All residues have main-chain dihedral angles in allowable regions of ϕ/ψ space with 90.0% in the most favored region (Figure 1). The final model consists of residues 1-101 and 114-164, two sulfate ions, and 87 water molecules. The side-chains of Asp115, Gln125, and Arg161 are modeled as alanine residues. The diffraction pat-

Table 1. Heavy-atom data statistics

Data set	Resolution (Å)	Reflections Measured	Reflections Unique	Completeness (%)	R_{sym}[a] (%)	MIFD[b] (%)	Phasing[c] power	R_{cullis}[d]
Native	2.7	18,740	4246	99.0	6.1			
$HgAc_2$	2.8	16,752	3801	99.0	6.6	27.0	1.94	0.67
EMTS	3.4	8994	2163	97.4	8.2	18.6	1.72	0.68
K_2PtCl_4	3.8	5056	1487	92.5	7.2	21.6	0.80	0.91
$K_2Pt(NO_2)_4$	3.8	8564	1573	97.0	8.8	21.1	0.70	0.92

[a] $R_{sym} = \Sigma|I_H - \langle i_H \rangle|/\Sigma i_H$, where $\langle I_h \rangle$ is the average over multiple observations.
[b] MIFD = Mean Isomorphous Difference, $\Sigma|F_{PH} - F_P|/\Sigma F_{PH}$ where F_{PH} and F_P are the derivative and native structure factor amplitudes, respectively.
[c] Phasing power = $|F_{H(calc)}|/||F_{PH(obs)} - F_{PH(calc)}||$.
[d] $R_{cullis} = \Sigma||F_{PH(obs)} \pm F_{P(obs)}| - F_{H(calc)}|/\Sigma|F_{PH(obs)} - F_{P(obs)}|$.

Table 2. Refinement statistics

A. *Data*	
Resolution (Å)	15-2.1
No. of reflections/unique	85,769/8216
Completeness (%)	96.9
R_{sym}	0.043
B. *Model*	
No. protein atoms	1237
No. solvent molecules	87 H_2O, 2 SO_4
Average *B*-factor (protein 1, H_2O); (Å^2)	39.4/47.7
R_{cryst} 15.0-2.1 Å	21.4
R_{free} 15.0-2.1 Å	25.0
rmsd bonds (Å)	0.01
rmsd angles (deg.)	1.4
rmsd *B*-factor (bonded atoms; Å^2)	1.9

terns of ovIFN-τ exhibit significant thermal diffuse scattering that is consistent with a highly mobile protein structure. Analysis of the electron density and individual *B*-factors shows that this flexibility is mainly located in the loop regions of ovIFN-τ. Representative electron density for residues in the core of the molecule and the loop regions are shown in Figure 2(a) and (b).

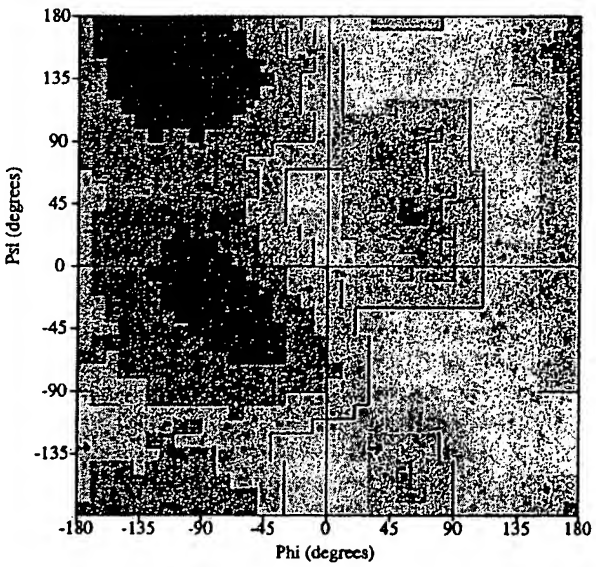

Figure 1. Ramachandran plot of the refined model of ovIFN-τ. The Figure was generated with the program Procheck (Laskowski *et al.*, 1993).

Structure of ovIFN-τ

OvIFN-τ is a monomer with overall dimensions of 20 Å × 30 Å × 40 Å (Figure 3). The molecule adopts a type I interferon fold that contains five α-helices (labeled A-E) which are linked by one overhand loop (Presnell & Cohen, 1989) the AB loop, and three shorter segments (BC, CD, and DE loops). Helices A, B, C, and E are antiparallel and tightly associated to form a left-handed four-helix bundle. Helix D runs approximately parallel with helix B and together with the extended portion of the AB loop packs against helices B and E. All five helices are relatively straight, with the exception of helix E that contains a 20° bend centered at Met148. This bend allows helix E to maximize its packing contacts with the rest of the helix bundle. The hydrophobic core of the molecule is predominantly made up of leucine residues. Several polar residues (Asn14, Ser64, Glu71, Gln92, Tyr123, Arg145, Ser155, Thr156, and Gln159) are buried in the molecular core. Five of these residues (Asn14, Gln92, Ser155, Thr156, and Gln159) form an extensive hydrogen bond network that includes two buried water molecules (Figure 2(a)).

The AB loop connects helix A and B. It is best described in three segments labeled the AB1 (residues 25-33), AB2 (residues 34-39), and AB3 (residues 40-52) loops. The BC, CD, and DE loops are made up of residues 75-79, 101-115, and 134-137, respectively. The AB1 loop is linked to helix E through a disulfide bond between Cys29 and Cys139. The AB2 loop runs parallel with the helix bundle and contributes Phe36 and Leu38 to the hydrophobic core of the molecule. Residues on the exposed surface of the loop form two stabilizing interactions. First, $O^{\delta 1}$ of Asp35 forms a hydrogen bond with the nitrogen atom of Gly37. Second, the main-chain oxygen of Leu38 forms a hydrogen bond with the $N^{\epsilon 2}$ atom of Gln40. The BC loop forms a solvent-accessible β-turn that places Trp77 away from the interior of the molecule. In the crystal, Trp77 packs into a hydrophobic pocket between helices A, C, and D of a symmetry related molecule (Figure 4). The hydrophobic pocket is formed by amino acid residues Cys1, Leu7, Phe54, Leu57, Leu96, Cys99, and Leu162. In other type I IFN structures, Trp77 packs into the hydrophobic core of the molecule near Trp141. The location of Trp77 in IFN-α_{2b}, as well as human and murine IFN-β is replaced by Glu71 in ovIFN-τ. The negatively charged glutamic acid residue forms a buried ion pair with Arg145. The high *B*-factors (~65 Å^2) observed for the BC loop suggest that it can adopt multiple conformations in solution. A notable feature of the DE loop is the left-handed α-helical conformations of Gly135 and Tyr136. This distinct loop structure places the O^{γ} atom of Ser137 in position to form a bifurcated hydrogen bond with the N atoms of Cys139 and Ala140 that form the first turn of helix E.

Although electron density is observed for the AB1, AB3, and BC loops, these loop regions have high *B*-factors and are presumed to adopt multiple conformations in solution. Each of these flexible residue segments are solvent exposed and found at the ends of the more rigid helix bundle. No electron density is observed for residues 102-113, and 165-172 located in the CD loop and C terminus, respectively. Analysis of ovIFN-τ crystals by MALDI-TOF mass spectroscopy revealed two broad peaks at 12,664.0 and 7255.5. These peaks likely correspond to ovIFN-τ peptide fragments 1-109 (calculated mass (cm) = 12,699) and 110-174 (cm = 7233.3), and suggest that the protein is being

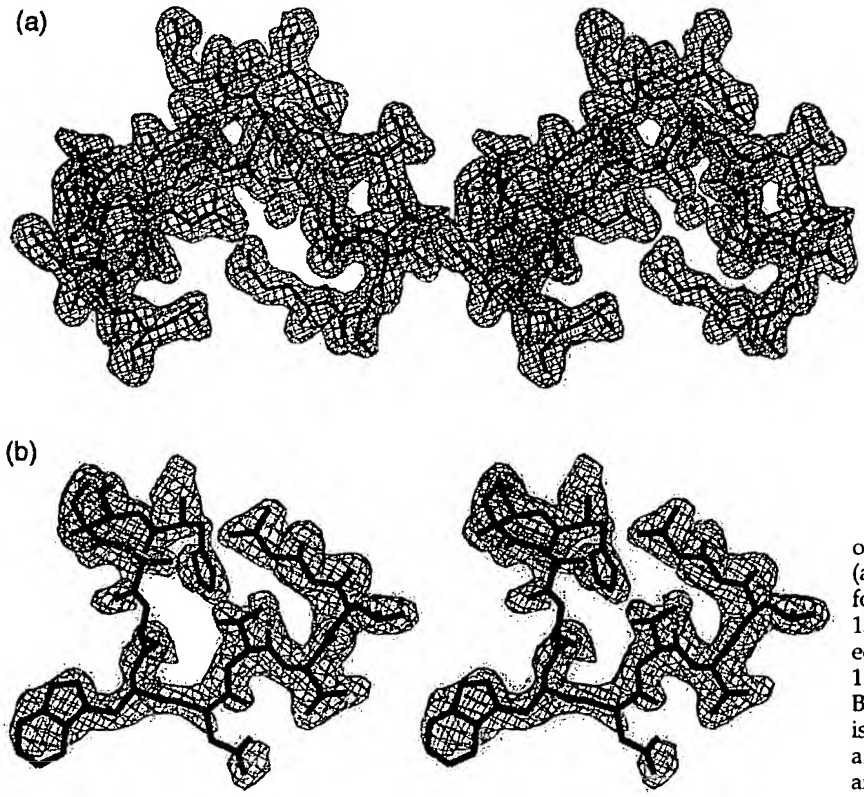

Figure 2. Stereoviews of the final ovIFN-τ electron density maps. (a) Final $2F_o - F_c$ electron density for helical residues 10-15, 89-96, 152-159 and two buried water molecules. The density is contoured at 1.0σ. (b) Final $2F_o - F_c$ density for BC loop residues 72-82. The density is contoured at 0.75σ. Carbon atoms are shown in green, oxygen in red, and nitrogen in blue.

cleaved in the CD loop between Asp109 and Ser110 during the extended crystallization experiment (six weeks). Additional cut sites in the CD loop are predicted from the identification of additional peaks that correspond to the ovIFN-τ fragments 1-106/107-172 and 1-112/113-172. Interestingly, mass spectroscopy on fresh crystallization drops revealed two peaks of 19,992.0 and 20,076.0 which corresponds to ovIFN-τ (cm = 19,914.5) plus one (cm = 19,994.5) or two (cm = 20,074.5) sulfate ions. This data provides a plausible reason for the lack of electron density for residues in the CD loop and also strengthens our interpretation of two large density peaks as sulfate ions. Adjacent to the disordered C terminus, well-defined electron density is observed for the N terminus of the molecule.

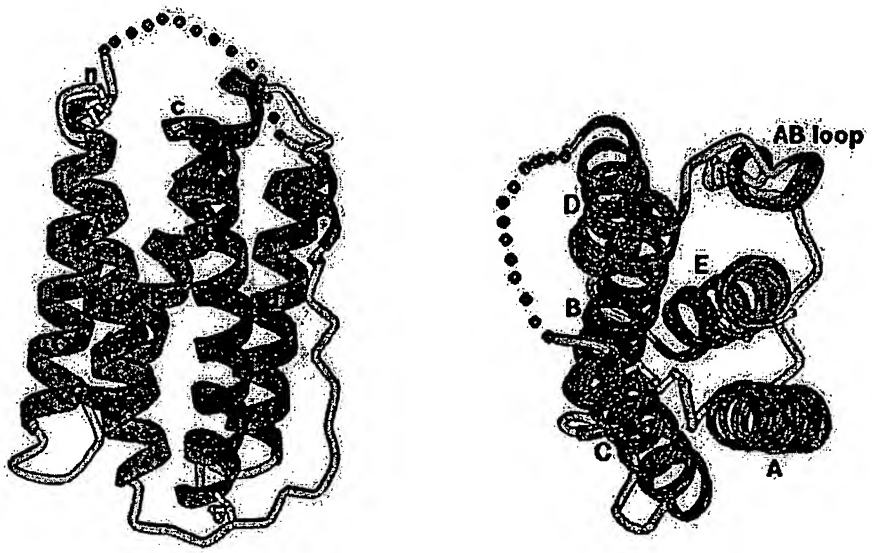

Figure 3. Ribbon diagram of ovIFN-τ. Two views are shown at 90° to one another. Helices are colored cyan and loops yellow. The CD loop not observed in the electron density map is denoted with red spheres for clarity.

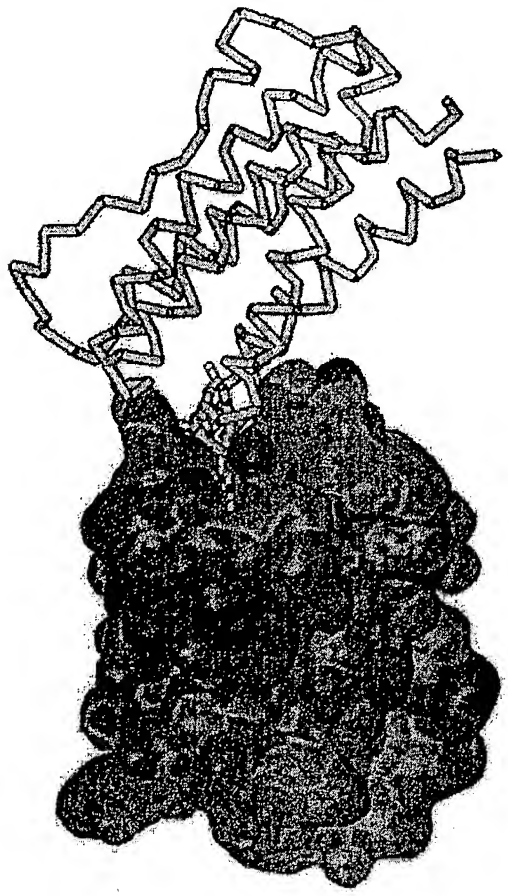

Figure 4. Crystal packing environment of Trp77. One ovIFN-τ molecule is represented as an accessible surface. Surface accessible carbon, oxygen, and nitrogen atoms are represented by green, red, and blue surfaces, respectively. A symmetry-related ovIFN-τ molecule is represented by C^{α} atoms. All atoms are shown for residues 75-80 of this molecule.

A second disulfide is found between Cys1 and Cys99 and links the N terminus to helix C. The fifth unpaired cysteine residue in ovIFN-τ (Cys86) is located on helix C where it is partially buried in the core of the molecule.

Conserved structural core of the type I IFNs

The overall fold of ovIFN-τ and IFN-α_{2b} are similar; 141 C^{α} atoms can be superimposed with a root-mean-square difference (rmsd) of 2.9 Å (Figure 5). Outliers in the superposition, C^{α} atoms that differ by more than 3 Å, are residues 6-7 at the N terminus, 23-32 in helix A and the AB1 loop, 49-52 in the AB3 loop, 71-77 in helix B and the BC loop, and 158-159 in helix E. The rmsd for the remaining 111 residue pairs is 1.2 Å. The C^{α} atom comparisons between ovIFN-τ and human and murine IFN-β yield overall rmsd values of ~3 Å for 140 residue pairs. Excluding C^{α} atom outliers greater that 3 Å results in a rmsd of ~1.3 Å for 114 atom pairs. The comparisons reveal a common conserved structural core (C^{α} differences less than 2 Å) between ovIFN-τ, huIFN-α_{2b}, huIFN-β, and muIFN-β, which consists of helix A (residues 8-21), AB2 loop (residues 34-39), helix B (residues 53-68), helix C (residues 79-100), and helices D and E (residues 117-155).

Comparison with IFN-α_{2b}

Helix A is eight residues longer in ovIFN-τ (residues 4-24) than in IFN-α_{2b} (residues 9-21). The C-terminal extension of helix A in ovIFN-τ, results in C^{α} atom differences of more than 6 Å for residues 23-25 (Figure 6). These structural changes result in new side-chain hydrogen bonds between $O^{\delta 1}$ and $N^{\delta 2}$ atoms of Asn22 with the O and NH1 atoms of Arg145 and between the O^{γ} of Ser25 with the $O^{\varepsilon 2}$ atom of Glu142. Relative to IFN-α_{2b}, the side-chain of Arg145 moves 5 Å towards the interior of the molecule. Additional differences in side-chain positions between ovIFN-τ and IFN-α_{2b} occur for Arg23 (~16 Å) and Leu24 (~11 Å). These large movements reflect the reverse orientations of Arg23 and Leu24 which point at the BC loop in IFN-α_{2b} and into the solvent near helix A in ovIFN-τ. Extension of helix A shortens the AB1 loop by two residues in ovIFN-τ and leads to main-chain differences with IFN-α_{2b} of up to 11 Å.

Additional differences of about 6 Å occur in helix B. Helix B is straight in ovIFN-τ and exhibits a 70° kink in IFN-α_{2b}. Four residues in IFN-α_{2b} (Ser69, Lys71, Asp72, and Tyr86) and ovIFN-τ (Tyr69, Glu71, His72, and Cys86) participate in different interactions that stabilize helix B in the kinked or straight conformation (Figure 7). The α-helical hydrogen bond pattern is disrupted by the kink in helix B of IFN-α_{2b}. Substitute hydrogen bonds to the exposed carbonyl oxygen atoms of helix B are formed by the side-chains of Ser69 and Tyr86. The position of the bulky Tyr86 side-chain in IFN-α_{2b} provides an additional steric constraint that promotes the kink in helix B. Tyrosine 69 and Cys86 in ovIFN-τ remove the hydrogen bonding and steric constraints provided by Ser69 and Tyr86 in huIFN-α_{2b}. An additional hydrogen bond is formed in ovIFN-τ between His72 of helix B and Glu83 on helix C.

The kink in helix B allows the BC loop of IFN-α_{2b} to pack tightly against the end of the helix bundle, while the straight extension of helix B observed in ovIFN-τ extends the BC loop away from the molecule. These differences significantly change the accessibility of residues located on helix B and the BC loop. In particular, the C^{α} position of Trp77 moves by 8.5 Å and does not pack against Trp141 in the interior of the protein as found for IFN-α_{2b} (Radhakrishnan *et al.*, 1996). The side-chain location of Trp77 in huIFN-α_{2b} is replaced by Glu71 in ovIFN-τ where it forms a buried salt bridge with Arg145. The buried environment of Glu71 in ovIFN-τ, was unexpected, since Lys71 is fully solvent exposed in huIFN-α_{2b} (Figure 7). The

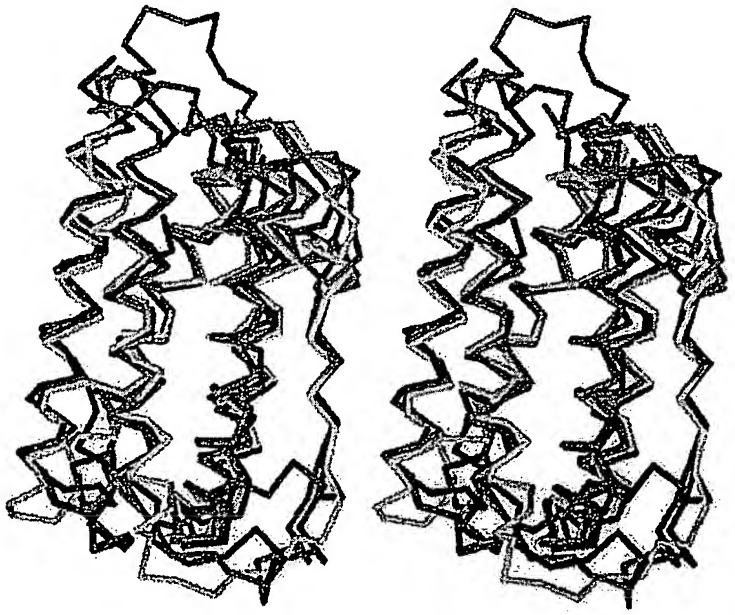

Figure 5. Stereoview comparison of the type I interferon structures. Only C^{α} atoms of ovIFN-τ (gold), huIFN-α_{2b} (green), huIFN-β (red), and muIFN-β (cyan) are shown.

distance between the C^{α} atom of Glu71 in ovIFN-τ and Lys71 in huIFN-α_{2b} is about 6 Å.

The conformation of helix B (straight or kinked) depends on the amino acid residues found at positions 69, 71, 72, and 86. Besides other ovIFN-τ sequences, the ovIFN-τ residue pattern (Tyr69, Glu71, His72, Cys86) is not strictly conserved in the type I IFN sequences (Figure 8). On the other hand, the residue pattern found in huIFN-α_{2b} (Ser69, Lys71, Asp 72, Tyr86) is observed in human subtypes IFN-α_2, IFN-α_5, IFN-α_6, IFN-α_8, and IFN-α_{16}. Interestingly, a subset of human IFN-α subtypes IFN-α_4, IFN-α_7, IFN-α_C, and IFN-α_{17}, have a Glu at position 71 and a Ser rather than Cys at position 86 as observed in ovIFN-τ. For huIFN-ω (His69, Glu71, Arg72, His86), only Glu71 is conserved with ovIFN-τ.

Structural differences between ovIFN-τ and huIFN-α_{2b} at the C-terminal end of helix E reflect the 20° bend which is found in helix E of ovIFN-τ, but not in huIFN-α_{2b}. The structural differences in helix E are influenced by Ser151 which, along with Glu147, forms a bifurcated hydrogen bond with Tyr123 in huIFN-α_{2b} (Radhakrishnan *et al.*, 1996). In ovIFN-τ, Ser151 is replaced by an alanine. Consistent with the Ser → Ala substitution, helix E in ovIFN-τ rotates clockwise ~20° (looking down the helix axis from the C terminus) which packs the methyl group of the alanine into the hydrophobic core of the molecule. Despite the rotation, C^{α} atom differences greater than 3 Å do not occur until residues 158-159. In this region of ovIFN-τ, hydrogen bonds are formed between the $O^{\varepsilon 1}$ and $N^{\varepsilon 2}$ of Gln 159 with the $N^{\varepsilon 2}$ of Gln92 and the O of Leu7 (Figure 2(a)). These interactions are not observed in huIFN-α_{2b}. Helix E is three amino acid residues longer in ovIFN-τ compared to helix E in huIFN-α_{2b}. Residues following Lys164 in ovIFN-τ and Glu160 in huIFN-α_{2b} are not observed and presumed to be flexible.

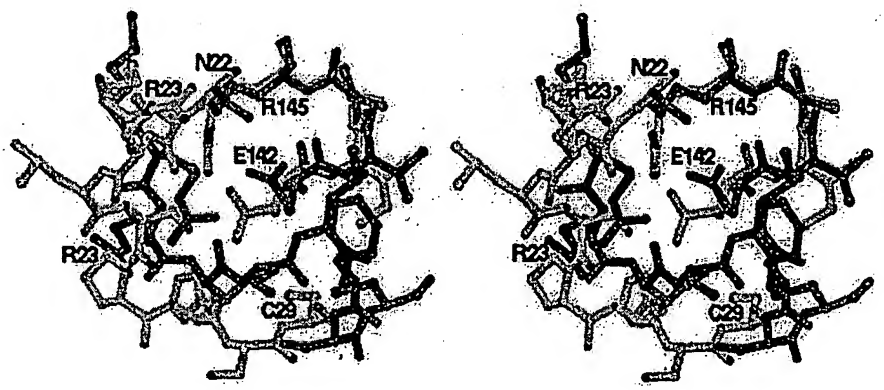

Figure 6. Stereoview comparison of helix A and the AB1 loop between ovIFN-τ (gold) and huIFN-α_{2b} (cyan). Residues 21-29 and 142-145 are shown. Oxygen and nitrogen atoms are colored red and blue, respectively. Selected residues are labeled.

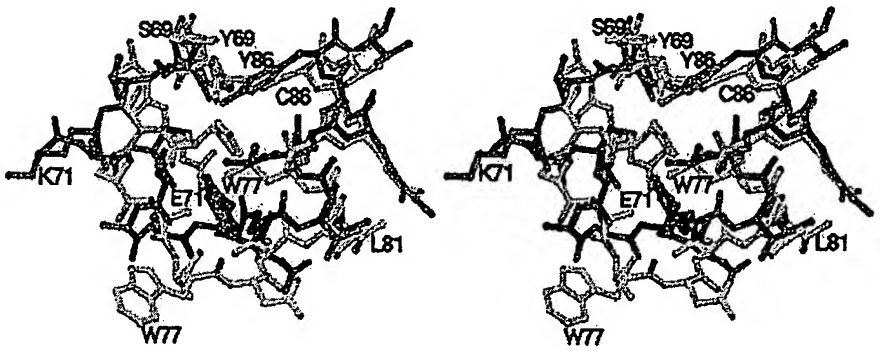

Figure 7. Stereoview comparison of helix B and the BC loop between ovIFN-τ (gold) and huIFN-α_{2b} (cyan). Residues 67-87 are shown. Oxygen and nitrogen atoms are colored red and blue, respectively. For clarity, the side-chains of residues 67, 68, and 85 have been removed from the Figure. Selected residues are labeled.

Discussion

In contrast to the zinc mediated dimers observed for human IFN-α_{2b} (Radhakrishnan *et al.*, 1996) and IFN-β (Karpusas *et al.*, 1997), ovIFN-τ is a monomer in the crystal. Superposition of ovIFN-τ, huIFN-α_{2b}, huIFN-β, and muIFN-β monomers, which display 30-50% sequence identity, reveals a conserved structural core of five α-helices and the AB2 loop. Regions that display the largest structural variations are also conserved. The greatest differences in C^{α} atom positions (~6-11 Å) occur in helix A, the AB1 loop, helix B, and the BC loop. These structurally variable regions are located on one end of the helix bundle where they likely play a significant role in the different functional properties of all type I IFNs. The structural differences in the loops are controlled by differences in the lengths and packing of the helices with few interactions within the middle of the loops. Furthermore, the hydrogen bond network between Asn22 (helix A), Arg145 (helix E) and Glu71 (helix B) provides a structural mechanism by which receptor binding at the AB1 loop may result in conformational changes to the BC loop.

OvIFN-τ and huIFN-α_2 compete for the same receptors on human and bovine cells and are predicted to share similar receptor binding sites (Subramaniam *et al.*, 1995; Li & Roberts, 1994a). The observed structural differences in helix A and the AB loop between ovIFN-τ and huIFN-α_{2b} (residues 1-8 and 22-32) occur in regions implicated in the differential receptor recognition and/or biological activity of ovIFN-τ and IFN-α_2. Specifically, hybrid scanning studies have shown that sequence differences within residues 16-28 are responsible for ~50-fold differences in activity between huIFN-α_1 and huIFN-α_2 on human cells (Weber *et al.*, 1987). Furthermore, an ovIFN-τ synthetic peptide (residues 1-37) was found to inhibit the antiviral activity of ovIFN-τ, but not huIFN-α_2, on MDBK cells (Pontzer *et al.*, 1994).

Despite the significant structural changes in helix B and the BC loop (residues 71-79) between ovIFN-τ and huIFN-α_{2b}, mutational analysis has mostly identified the exposed residues of helix C (residues 80, 84, 86, and 90) in receptor binding and altered biological activity (Uzé *et al.*, 1994). This apparent discrepancy may be explained by the unique hydrogen-bonding networks observed in the straight (ovIFN-τ) or kinked (huIFN-α_{2b}) conformation of helix B. In particular, Tyr86 participates in important Van der Waal's and hydrogen bond interactions that stabilize helix B in the bent conformation in IFN-α_{2b}. A similar structural role for tyrosine residues has been observed in the bent helices of the related cytokines IL-10 and IFN-γ (Walter & Nagabhushan, 1995). Hybrid studies have shown that sequence differences between IFN-α_1 and IFN-α_2 at positions Ser69 → Thr, Thr 80 → Asp, and Tyr86 → Cys cause a reduction of IFN-α_2 activity on human cells, while simultaneously increasing its activity on murine cells (Rehberg *et al.*, 1982). Substitution of Tyr86 with Cys is required to obtain the straight helix B and flexible BC loop observed in ovIFN-τ. Thus, the Tyr86 → Cys substitution on helix C in the IFN-α chimera may also result in conformational changes to residues 71-79.

The presence of Glu71 and Ser86 in the human IFN-α_4, IFN-α_7, IFN-α_C and IFN-α_{17} suggests that these four human subtypes adopt an extended helix B and BC loop conformation similar to ovIFN-τ. Additional non-conservative amino acid residue differences between the four subtypes and IFN-α_{2b} occur in helix A and helix E. Each residue is located in helices that display significant structural differences in ovIFN-τ and huIFN-α_{2b}. For huIFN-α_{2b}, Arg22 is replaced by Gly22 in each of the four subtypes. Furthermore, residue position 160 is a Glu in huIFN-α_{2b} and a Lys in ovIFN-τ, IFN-α_4, IFN-α_7, IFN-α_C and IFN-α_{17}. Neither Glu160 in huIFN-α_{2b} nor Lys160 in ovIFN-τ plays a role in stabilizing the conformation of helix E. Consistent with the predicted similarities of ovIFN-τ and huIFN-α_4, deletion of 11 residues from the C terminus of ovIFN-τ or eight residues from the C terminus of IFN-α_4 reduces antiviral activity to a greater extent than removing 11 resi-

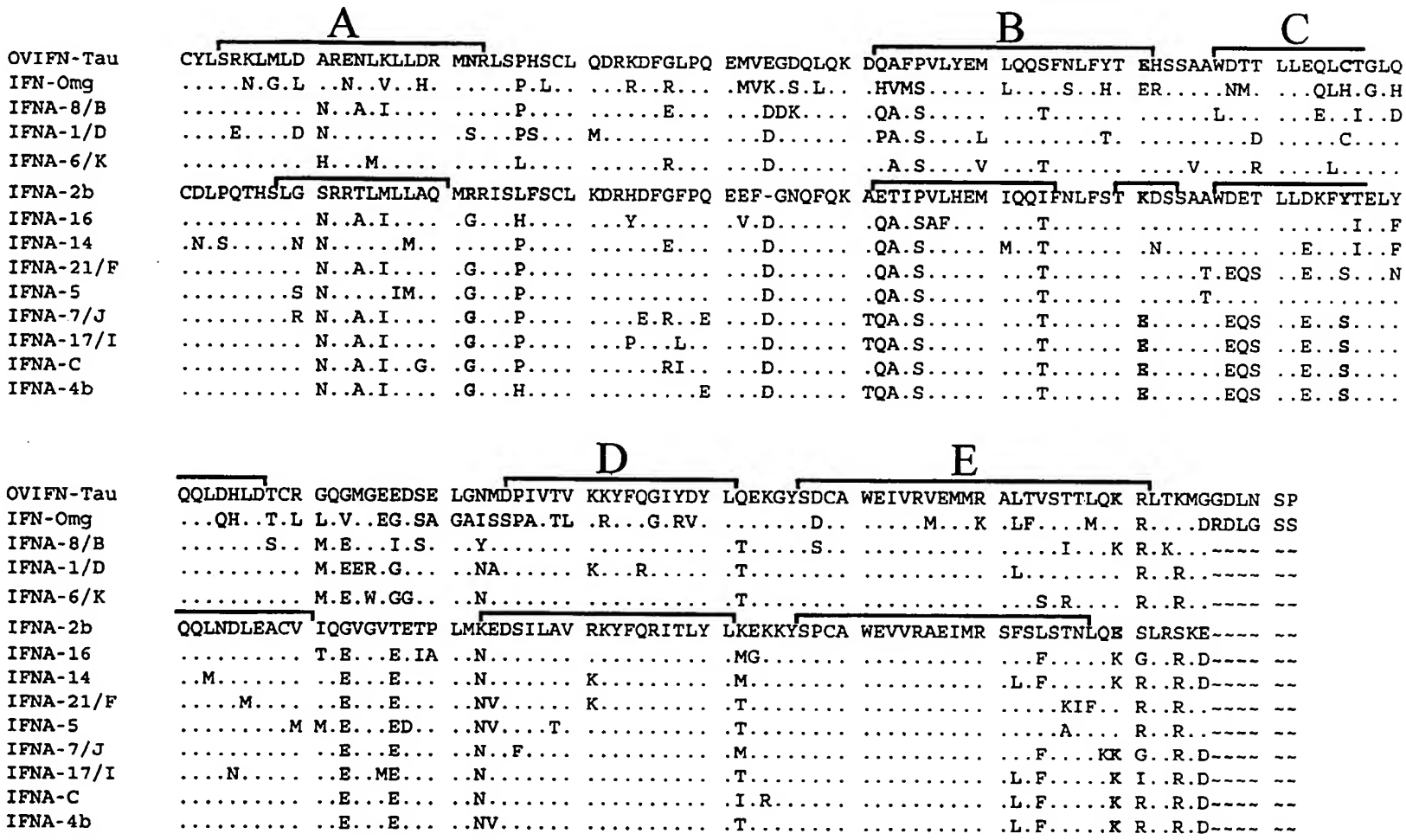

Figure 8. Amino acid sequence alignment of ovIFN-τ, huIFN-ω, and the 12 human IFN-α subtypes (Pestka, 1997). Residues are shown in blocks of ten. The location of the α-helices for ovIFN-τ and huIFN-α_{2b} are shown as black bars. All residues are shown for ovIFN-τ and huIFN-α_{2b}. For other sequences, a period is shown for residues with sequence identity to huIFN-α_{2b}. Residues 22, 71, 86, and 160 that were identified as markers of the structural differences between ovIFN-τ and huIFN-α_{2b} and are conserved among human IFN-α subtypes α_7, α_{17}, α_c and α_{4b} are in bold type.

dues from the C terminus of IFN-α_2 (Li & Roberts, 1994b; Cheetham *et al.*, 1991; Chang *et al.*, 1983).

The IFNAR-2 has been shown to bind several human IFN-α subtypes as well as IFN-β, while the IFNAR-1, although required for biological activity, plays only a complementary role in ligand binding affinity (Cohen *et al.*, 1995). Structure-function studies with human IFN-α suggest that the IFNAR-1 binding site is made up of exposed residues on helix A and C (Uzé *et al.*, 1994). On the opposite side of the molecule, the IFNAR-2 binding site is predicted to consist of a group of highly conserved residues on the AB loop, helix D, and the DE loop (Mitsui *et al.*, 1993). Despite crystal structures for growth hormone and IFN-γ receptor complexes (de Vos *et al.*, 1991; Walter *et al.*, 1995), attempts to construct a plausible IFN-α receptor complex model that explains all of the structure-function data has not been accomplished. This may reflect yet unidentified interactions between the type I IFNs and their receptors, or be the result of miss-interpreting the structural consequences of various mutational data. The complexities of interpreting structure-function data in the type I IFN system arise from the potential biological importance of IFN-α and IFN-β dimers (Radhakrishnan *et al.*, 1996; Karpusas *et al.*, 1997), novel splice variants for the IFNAR-1 (Cook *et al.*, 1996), and the recent identification of at least one additional receptor chain on human T cells (Petricoin *et al.*, 1997).

The crystal structure of ovIFN-τ provides information on the conformational variability of the type I IFNs. The location of structurally conserved and variable regions between ovIFN-τ and huIFN-α_{2b} is consistent with the functional properties and proposed binding sites of the known IFN-α receptors. For example, the requirement of the IFNAR-2 to bind a common site on all type I IFNs is supported by the low rmsd (0.4 Å, residues 34-41 and 115-149) between ovIFN-τ and huIFN-α_{2b} in the proposed IFNAR-2 binding site. In contrast, larger structural changes (0.8 Å, residues 8-22 and 80-100) are observed between ovIFN-τ and huIFN-α_{2b} in helix A, which along with helix C is proposed to interact with the signal transducing IFNAR-1. The large structural differences between ovIFN-τ and huIFN-α_{2b} in helix B and the BC loop suggest that they are important for receptor binding, although little biochemical evidence is currently available in the human IFN-α system. The structural differences in this region may be involved in the unique function of ovIFN-τ as a pregnancy recognition hormone. The close proximity of helix B and the BC loop to helix C suggests that it could also form part of the IFNAR-1 binding site. Additional mutagenesis studies with purified receptor components as well as a crystal structure of a type I IFN receptor complex will be required to answer these questions.

Materials and Methods

Crystallization

Recombinant ovIFN-τ was expressed in yeast (*Pichia pastoris*) and purified as described (Ott *et al.*, 1991). The purified protein was crystallized by hanging-drop vapor diffusion techniques. The protein drops consisted of 1 μl of ovIFN-τ solution (20 mg/ml) and 1 μl of the reservoir solution consisting of 0.8 M $LiSO_4$, 100 mM citrate buffer (pH 4.8). The drops were equilibrated over 1 ml of reservoir solution at room temperature. Crystals, with maximum dimensions of 0.35 mm^3, were obtained after about six weeks. The crystals belong to the orthorhombic space group $P2_12_12_1$ with unit cell dimensions of $a = 39.30$ Å, $b = 45.60$ Å, and $c = 75.84$ Å. The crystals contain one molecule in the asymmetric unit which corresponds to a solvent content of about 27% (Matthews, 1968). Mass analysis of ovIFN-τ crystals was carried out on a Voyager Elite mass spectrometer with delayed extraction technology (PerSeptive Biosystems, Framingham, MA) operating in the positive mode. The acceleration voltage was set at 25 kV and 50-100 laser shots were summed. Samples were mixed 1:10 with Sinapinic acid dissolved in acetonitrile:0.1% (v/v) trifluoroacetic acid (1:1). Apomyoglobin was used as an internal standard.

X-ray data collection and MIR phasing

Intensity data were collected using a R-AXIS IV image plate detector using CuKα radiation ($\lambda = 1.5418$ Å) from a Rigaku RU-200 rotating anode generator (50 kV, 100 mA) equipped with focusing mirrors (MSC, The Woodlands, Texas). Initial native and heavy-atom derivative datasets were collected at room temperature (Table 1). A final native dataset was collected at −170°C (Table 2). Crystals were prepared for low temperature data collection by equilibration in a cryoprotectant solution containing 20% (v/v) glycerol, 1.4 M $LiSO_4$, and 100 mM citrate buffer (pH 4.8). Data were integrated and scaled using the programs DENZO and SCALEPACK (Otwinowski, 1993). All multiple isomorphous replacement calculations were performed using the CCP4 suite of programs (CCP4, 1994). The single site $HgAc_2$ and EMTS derivatives were identified by inspection of difference Patterson maps. Two additional weak derivatives (K_2PtCl_4 and $K_2Pt(NO_2)_4$) were identified by mercury cross-phased difference Fourier maps. Despite their poor statistics, maps calculated with these two additional derivatives were of better quality than the two derivative maps. Heavy-atom refinement and subsequent phase calculations were carried out in MLPHARE (Table 1; Otwinowski, 1991). MIR phases were calculated at 2.8 Å and anomalous data were included for the $HgAc_2$ derivative. The phases were further improved by solvent leveling and histogram matching procedures in DM (Cowtan, 1994). The resulting DM modified electron density map displayed well-defined α-helices corresponding to residues 4-23, 56-72, 81-99, and 122-160. Alignment of the sequence to the map was facilitated by the model of recombinant human IFN-α_{2b} (PDB entry 1RH2). Model building was done using the interactive graphics programs TOM (Cambillau & Horjales, 1987) and O (Jones & Kjeldgaard, 1993). Confidence in the sequence alignment was obtained by the overall agreement of the side-chain electron density for each ovIFN-τ residue. In addition, the heavy-atom sites were located close to ovIFN-τ side-chains that had affinity for that particular metal ion.

Structure refinement

Initial refinements were done using X-PLOR 3.8.5 (Brunger, 1991) using the stereochemical parameter files defined by Engh & Huber (1991). Prior to refinement, 10% of the data were randomly omitted for monitoring the free *R*-factor (Brunger, 1992). The initial model was subjected to four cycles of simulated annealing using X-PLOR, SIGMAA weighting, and phase combination (Read, 1986) which resulted in an R_{free} of 31.9%. Additional torsion angle dynamic refinement (Rice & Brunger, 1997) was carried out using the maximum likelihood target function (Pannu & Read, 1996) as implemented in CNS (Brunger *et al.*, 1998). CNS refinements included corrections for the bulk solvent and anisotropy in the diffraction data (Jiang & Brunger, 1994). The stereochemical quality of the ovIFN-τ model at all stages in the refinement was monitored using PROCHECK (Laskowski *et al.*, 1993). Model superpositions were performed manually using the computer graphics and improved by least squares (Kabsch, 1976). Amino acid sequence alignments were performed using the GCG computer package (Wisconsin Package Version 9.0). For comparison, residues in ovIFN-τ and IFN-α_{2b} were numbered according to the consensus IFN sequence which counts the deletion at position 44. The graphics program CHAIN was used to generate Figure 2 (Sack, 1988). The RIBBONS program suite was used to generate Figures 3-7 (Carson, 1991)

Protein Data Bank accession number

OvIFN-τ coordinates and structure factors have been deposited in the Brookhaven Protein Data Bank accession nos 1b51 and 1b51sb.

Acknowledgments

We thank Maxine Rice and Jun Dai for help in manuscript preparation, and Lori Coward in the UAB Comprehensive Cancer Center for MALDI-TOF mass spectroscopy. This work was supported in part by grants to M.R.W. from the American Heart Association (Grant no. 96008020) and the NIH (Grant no. AI36871), and to H.M.J. through NIH grant no. CA69959.

References

Abdel-Meguid, S. S., Shieh, H.-S., Smith, W. W., Dayringer, H. E., Violand, B. N. & Bentle, L. A. (1987). Three-dimensional structure of a genetically engineered variant of porcine growth hormone. *Proc. Natl Acad. Sci. USA*, **84**, 6434-6437.

Barbieri, G., Velazquez, L., Scrobogna, M., Fellous, M. & Pellegrin, S. (1994). Activation of the protein tyrosine kinase tyk2 by interferon α/β. *Eur. J. Biochem.* **232**, 427-435.

Baron, S., Tyring, S. K., Fleischmann, W. R., Coppenhaver, D. H., Neisel, D. W., Klimpel, G. R., Stanton, G. J. & Hughes, T. K. (1991). Mechanisms of action and clinical applications. *J. Am. Med. Assoc.* **266(10)**, 1375-1383.

Brunger, A. T. (1991). *X-PLOR, Manual Version 3.1*, Yale University Press, New Haven, CT.

Brunger, A. T. (1992). Free R value: a novel statistical quantity for assessing the accuracy of crystal structures. *Nature*, **355**, 472-475.

Brunger, A. T., Adams, P. D., Clore, G. M., DeLano, W. L., Gros, P., Grosse-Kunstleve, W., Jian, J., Kuszewski, J., Nilges, M., Pannu, N. S., Read, R. J., Rice, L. M., Simonson, T. & Warren, G. L. (1998). Crystallography and NMR system (CNS): a new software suite for macromolecular structure determination. *Acta. Crystallog. sect. D*, **54**, 905-921.

Cambillau, C. & Horjales, E. (1987). TOM: a FRODO subpackage for protein-ligand fitting with interactive energy minimization. *J. Mol. Graph*, **5**, 175-177.

Carson, M. (1991). Ribbons 2. 0. *J. Appl. Crystallog.* **24**, 958-961.

CCP4. (1994). The CCP4 Suite: programs for protein crystallography. *Acta Crystallog. sect. D*, **50**, 760-763.

Chang, N. T., Kung, H-F. & Pestka, S. (1983). Synthesis of a human leukocyte interferon with a modified carboxy terminus in *Escherichia coli*. *Arch. Biochem. Biophys.* **221(2)**, 585-589.

Cheetham, B. F., McInnes, B., Mantamadiotis, T., Murray, P. J., Ålin Per Bourke, P., Linnane, A. W. & Tymms, M. J. (1991). Structure-function studies of human interferon-α: enhanced activity on human and murine cells. *Antiviral Res.* **15**, 27-40.

Cohen, B., Novick, D., Barak, S. & Rubinstein, M. (1995). Ligand-induced association of the type I interferon receptor components. *Mol. Cell. Biol.* **15**, 4208-4214.

Colamonici, O. R., Platanias, L. C., Domanski, P., Handa, R., Gilmour, K. C., Diaz, M. O., Reich, N. & Pitha-Rowe, P. (1996). Transmembrane signaling by the α subunit of the type I interferon receptor is essential for activation of the jak kinases and the transcriptional factor ISGF3. *J. Biol. Chem.* **270(14)**, 8188-8193.

Cook, J. R., Cleary, C. M., Mariano, T. M., Izotova, L. & Pestka, S. (1996). Differential responsiveness of a splice variant of the human type I interferon receptor to interferons. *J. Biol. Chem.* **271(23)**, 13448-13453.

Cowtan, K. (1994). 'DM' an automated procedure for phase improvement by density modification. In *Joint CCP4 and ESF: EACBM Newsletter on Protein Crystallography* (Bailey, S. & Wilson, K., eds), vol. 31, pp. 34-38, Dansbury Laboratory, Hamburg, Germany.

de Vos, A. M., Ultsch, M. & Kossiakoff, A. A. (1991). Human growth hormone and extracellular domain of its receptor: crystal structure of the complex. *Science*, **255**, 306-312.

Domanski, P., Witte, M., Kellum, M., Rubinstein, M., Hackett, R., Pitha, P. & Colmonici, (1995). Cloning and expression of a long form of the β subunit of the interferon αβ receptor that is required for signaling. *J. Biol. Chem.* **270(37)**, 21606-21611.

Engh, R. A. & Huber, R. (1991). Accurate bond and angle parameters for X-ray protein structure refinement. *Acta Crystallog. sect. A*, **47**, 392-400.

Godkin, J. D., Bazer, F. W., Moffatt, J., Sessions, F. & Roberts, R. M. (1982). Purification and properties of a major, low molecular weight protein released by the trophoblast of sheep blastocysts at Day 13-21. *J. Reprod. Fert.* **65**, 141-150.

Imakawa, K., Anthony, R. V., Kazemin, M., Marotti, K. R., Polites, H. G. & Roberts, R. M. (1987). Interferon-like sequence of ovine trophoblast protein secreted by embryonic trophectoderm. *Nature*, **330**, 377-379.

Jarpe, M. A., Johnson, H. M., Bazer, F. W., Ott, T. L., Curto, E. V., Krishna, N. R. & Pontzer, C. H. (1994). Predicted structural motif of IFNτ. *Protein Eng.* 7(7), 863-867.

Jiang, J.-S. & Brunger, A. T. (1994). Protein hydration observed by X-ray diffraction. Solvation properties of penicillopepsin and neuraminidase crystal structures. *J. Mol. Biol.* 243, 100-115.

Jones, A. T. & Kjeldgaard, M. (1993). *O-The Manual, Version 5.9*, Uppsala, Sweden.

Kabsch, W. (1976). A solution of the best rotation to relate two sets of vectors. *Acta Crystallog. sect. A*, 32, 922-923.

Karpusas, M., Nolte, M., Benton, C. B., Meier, W., Lipscomb, W. N. & Goelz, S. (1997). The crystal structure of human interferon β at 2.2-Å resolution. *Proc. Natl Acad. Sci. USA*, 94, 11813-11818.

Laskowski, R. J., Macarthur, M. W., Moss, D. S. & Thronton, J. M. (1993). Procheck: a program to check sterochemical quality of protein structures. *J. Appl. Crystallog.* 26, 283-290.

Li, J. & Roberts, R. M. (1994a). Structure-function relationships in the interferon-τ (IFN-τ). *J. Biol. Chem*, 269, (18), 13544-13550.

Li, J. & Roberts, R. M. (1994b). Interferon-τ and interferon-α interact with the same receptors in bovine endometroium. *J. Biol. Chem.* 269(40), 24826-24833.

Matthews, B. W. (1968). Solvent content of protein crystals. *J. Mol. Biol.* 33, 491-497.

Mitsui, Y., Senda, T., Shimazu, T., Matsuda, S. & Utsumi, J. (1993). Structural, functional and evolutionary implications of the three-dimensional crystal structure of murine interferon-β. *Pharmacol. Ther.* 58, 93-132.

Nagabhushan, T. L. & Giaquinto, A. (1995). *Biopharmaceutical Production* (Lubiniecki, A. S. & Vargo, S. A., eds), pp. 221-234, John Wiley & Sons, New York, NY.

Navaza, J. (1994). AMoRe: an automated package for molecular replacement. *Acta Crystallog. sect. A*, 50, 157-163.

Ott, T. L., Van Heeke, G., Johnson, H. M. & Bazer, F. W. (1991). Cloning and expression in *Saccharomyces cerevisiae* of a synthetic gene for the type-I trophoblast interferon ovine trophoblast protein-1: purification and antiviral activity. *J. Interferon Res.* 11, 357-364.

Otwinowski, Z. (1991). Maximum likehood refinement of heavy-atom parameters. In *Isomorphous Replacement and Anomalous Scatterings: Proceedings of the CCP4 Study Weekend* (Wolf, W., Evan, P. R. & Leslie, A. G. W., eds), pp. 23-38.

Otwinowski, Z. (1993). Oscillation data reduction program. In *Data Collection and Processing: Proceedings of the CCP4 Study Weekend* (Sawyer, L., Isaacs, N. & Bailey, S., eds).

Pannu, N. S. & Read, R. J. (1996). Improved structure refinement through maximum likelihood. *Acta Crystallog. sect. A*, 52, 659-668.

Pellegrini, S. & Dusanter-Fourt, I. (1997). The structure, regulation and function of the Janus kinases (JAKs) and the signal transducers and activators of transcription (STATs). *Eur. J. Biochem.* 248(3), 615-633.

Pestka, S. (1997). The human interferon-α species and hybrid proteins. *Semin. Oncol.* 24(S9), 4-17.

Petricoin, E. F., Ito, S., Williams, B. L., Audet, S., Stancato, L. F., Gamero, A., Clouse, K., Grimley, P., Weiss, A., Beeler, J., Finbloom, D. S., Shores, E. W., Abraham, R. & Larner, A. C. (1997). Antiproliferative action of interferon-a requires component of T-cell-receptor signalling. *Nature*, 390, 629-632.

Pontzer, C. H., Torres, B. A., Vallet, J. L., Bazer, F. W. & Johnson, H. M. (1988). Antiviral activity of the pregnancy recognition hormone ovine trophoblast protein-1. *Biochem. Biophys. Res. Commun.* 152(2), 801-807.

Pontzer, C. H., Ott, T. L., Bazer, F. W. & Johnson, H. M. (1990). Localization of an antiviral site on the pregnancy recognition hormone, oving trophoblast protein 1. *Proc. Natl Acad. Sci. USA*, 87, 5945-5949.

Pontzer, C. H., Bazer, F. W. & Johnson, H. M. (1991). Antiproliferative activity of a pregnancy recognition hormone, ovine trophoblast protein-1. *Cancer Res.* 51, 5304-5307.

Pontzer, C. H., Ott, T. L., Bazer, F. W. & Johnson, H. M. (1994). Structure/function studies with interferon tau: evidence for multiple active sites. *J. Interferon Res.* 14, 133-141.

Presnell, S. R. & Cohen, F. R. (1989). Topological distribution of four-alpha-helix bundles. *Proc. Natl Acad. Sci. USA*, 86, 6592-6596.

Radhakrishnan, R., Walter, L. J., Hruza, A., Reichert, P., Trotta, P. P., Nagabhushan, T. L. & Walter, M. R. (1996). Zinc mediated dimer of human interferon-α_{2b} revealed by X-ray crystallography. *Structure*, 4, 1453-1463.

Read, R. J. (1986). Improved fourier coefficients for maps using phases from partial structures with errors. *Acta Crystallog. sect. A*, 42, 140-149.

Rehberg, E., Kelder, B., Hoal, E. G. & Pestka, S. (1982). Specific molecular activities of recombinant and hybrid leukocyte interferons. *J. Biol. Chem.* 257, 11497-11502.

Rice, L. M. & Brunger, A. T. (1994). Torsion angle dynamics: reduced variable conformational sampling enhances crystallographic structure refinement. *Proteins: Struct. Funct. Genet.* 19, 277-290.

Roberts, R. M. (1991). A role for interferons in early pregnancy. *BioEssays*, 13(3), 121-126.

Roberts, R. M., Cross, J. C. & Leaman, D. W. (1991). Unique features of the trophoblast interferons. *Pharmacol. Ther.* 51, 329-345.

Roberts, R. M., Cross, J. C. & Leaman, D. W. (1992). Interferons as hormones of pregnancy. *Endocrine Rev.* 13, 432-452.

Sack, J. S. (1988). CHAIN: a crystallographic modeling package. *J. Mol. Graph.* 6, 224-225.

Senda, T., Saitoh, S.-I. & Mitsui, Y. (1995a). Refined crystal structure of recombinant murine interferon-β at 2.15 Å resolution. *J. Mol. Biol.* 253, 187-207.

Senda, T., Saitoh, S.-I., Mitsui, Y., Li, J. & Roberts, R. M. (1995b). A three-dimensional model of interferon-τ. *J. Interferon Res.* 15, 1053-106.

Seto, M. H., Harkins, R. N., Adler, M., Whitlow, M., Church, W. B. & Croze, E. (1995). Homology model of human interferon-α8 and its receptor complex. *Protein Sci.* 4, 655-670.

Sprang, S. & Bazan, J. F. (1993). Cytokines structural taxonomy and mechanisms of receptor engagement. *Curr. Opin. Struct. Biol.* 3, 815-827.

Strander, H. A. (1989). Clinical effects of interferon therapy with special emphasis on antitumor efficacy. *Acta Oncol.* 28, 355-362.

Subramaniam, P. S., Khan, S. A., Pontzer, C. H. & Johnson, H. M. (1995). Differential recognition of the type I interferon receptor by interferons τ and α is responsible for their disparate cytotoxicities. *Proc. Natl Acad. Sci. USA*, 92, 12270-12274.

Uzé, G., Luttalla, G. & Gresser, I. (1990). Genetic transfer of a functional human interferon α receptor into mouse cells: cloning and expression of its cDNA. *Cell*, **60**, 225-234.

Uzé, G., Di Marco, S., Mouchel-Vielh, E., Monneron, D., Bandu, M.-T., Horisberger, M. A., Dorques, A., Lutfalla, G. & Mogenson, K. E. (1994). Domains of interaction between alpha interferon and its receptor components. *J. Mol. Biol.* **243**, 245-257.

Walter, M. R. & Nagabhushan, T. L. (1995). Crystal structure of interleukin 10 reveals an interferon γ-like fold. *Biochemistry*, **34**, 12118-12125.

Walter, M. R., Windsor, W. T., Nagabhushan, T. L., Lundell, D. J., Lunn, C. A., Zauodny, P. J. & Narula, S. K. (1995). Crystal structure of a complex between interferon-γ and its soluble high-affinity receptor. *Nature*, **376**, 230-235.

Weber, H., Valenzuela, D., Lujber, G., Gubler, M. & Weissman, C. (1987). Single amino acid changes that render human IFN-α_2 biologically active on mouse cells. *EMBO J.* **6**, 591-598.

Wisconsin Package Version 9.0, Genetics Computer Group (GCG), Madison, Wisc.

Edited by R. Huber

(Received 10 June 1998; received in revised form 20 November 1998; accepted 3 December 1998)